Atmos. Chem. Phys. Discuss., 12, 14669–14695, 2012
www.atmos-chem-phys-discuss.net/12/14669/2012/
doi:10.5194/acpd-12-14669-2012

Atmospheric Chemistry and Physics Discussions

Chamber simulation of photooxidation of dimethyl sulfide and isoprene in the presence of NO_x

T. Chen and M. Jang

Department of Environmental Engineering Sciences, P.O. Box 116450, University of Florida, Gainesville, 32611 FL, USA

Received: 17 February 2012 – Accepted: 15 May 2012 – Published: 8 June 2012

Correspondence to: M. Jang (mjang@ufl.edu)

Published by Copernicus Publications on behalf of the European Geosciences Union.

Abstract

In the kinetic model of this study, to advance the photooxidation of dimethyl sulfide (DMS) in the gas phase, the most recently reported reactions with their rate constants have been included. To improve the model predictability for the formation of sulfuric acid and methanesulfonic acid (MSA), heterogeneous reactions of gaseous DMS products (e.g., dimethyl sulfoxide (DMSO)) on the surface of aerosol have been included in the kinetic model. DMS was photoirradiated in the presence of NO_x using a 2 m^3 Teflon film chamber. The resulting chamber data was simulated using the new kinetic model. The model included in this study predicted that concentrations of both MSA and H_2SO_4 would significantly increase due to heterogeneous chemistry and this was well substantiated with experimental data. The model used in this study also predicted the decay of DMS, the formation of other gaseous products such as SO_2, dimethyl sulfone ($DMSO_2$), and the ozone formation linked to a NO_x cycle. To study the effect of coexisting volatile organic compounds, the photooxidation of DMS in the presence of isoprene and NO_x has been simulated using the new kinetic model integrated with the Master Chemical Mechanism (MCM) for isoprene oxidation, and compared to chamber data. Both the model simulation and the experimental data showed an increase in the yields of MSA and H_2SO_4 as the isoprene concentration increased.

1 Introduction

Dimethyl sulfide (DMS) is a major reduced sulfur compound of marine origin. The major aerosol phase products of DMS are methanesulfonic acid (MSA) and sulfuric acid (Bardouki et al., 2003; Barone et al., 1995; Gaston et al., 2010; Lukács et al., 2009), both of which are postulated to have significant effects on the earth's radiation budget (Charlson et al., 1987). The Intergovernmental Panel on Climate Change (IPCC) has classified the aerosol originating from DMS as one of the most important components that needs to be better understood in the planetary climate system (IPCC, 1995). The

ACPD
12, 14669–14695, 2012

DMS photooxidation mechanism is an important factor for understanding the role DMS plays in the earth's sulfur cycle and climate system, so it has been studied by many researchers (Yin et al., 1990; Turnipseed and Ravishankara, 1993; Urbanski and Wine, 1999; Barnes et al., 2006).

Despite all the efforts exerted to understanding atmospheric DMS chemistry, a large discrepancy still exists between the ambient measurements of DMS products and the simulation results for compounds such as DMSO (Chen et al., 2000), H_2SO_4 and MSA (Lucas and Prinn, 2002). The poor predictability of the kinetic model for the formation of DMS products was caused by uncertainties in the rate constants of DMS reactions in the gas phase, the lack of aerosol phase reactions of the DMS products, and missing information regarding the impact of volatile organic compounds (VOC) on the DMS photooxidation through both the gas and the particle phases.

In the presence of UV light, DMS oxidation is initiated by OH· radical reactions through both the hydrogen (H) abstraction reaction and the addition reaction (Atkinson et al., 1989). It is known that DMS also reacts with $O(^3P)$, NO_3 (Atkinson et al., 1989) and NO_2 (Balla and Heicklen, 1984). The updated mechanisms and rate constants of the DMS initial reactions and sequential reactions have been included in Tables S1–3 of the supplementary materials. For example, the rate constant (s^{-1} molecules^{-1} cm^3) for the OH radical abstraction reaction of DMS (No. 59) was suggested to be $1.13 \times 10^{-11}\exp(-254/T)$ by Atkinson et al. (1997); the rate constant for the OH radical addition reaction to DMSO (No. 2) was updated to $6.1\times10^{-12}\exp(800/T)$ (Sander et al., 2006). Two other initial reactions of DMSO oxidation (No. 1 and 3) were newly added (Sander et al., 2006). The change of the reaction rate constants may influence both the prediction of the DMS decay and its product distribution.

The missing aerosol-phase reactions in the DMS mechanism is another reason why several important DMS products such as MSA and H_2SO_4 have been underpredicted using the existing model. Recent field studies indicate that the heterogeneous reactions of DMS products significantly contribute to the formation of MSA in the aerosol. For example, in a field study in the equatorial Pacific, Davis et al. (1999) indicated that

ACPD
12, 14669–14695, 2012

the production of MSA through gas to particle partitioning account for only 1 % of the observed aerosol phase MSA. Similarly, through an eastern Mediterranean campaign, Mihalopoulos et al. (2007) suggested that at least 80 % of the production of aerosol phase MSA may be due to heterogeneous reactions of DMS photooxidation products (possibly DMSO). Bardouki et al. (2002) confirmed that the liquid phase reactions of DMSO and MSIA with OH radicals produce MSA with high yields. To better predict the atmospheric fate of DMS, the development of an advanced kinetic model is needed.

The failure to consider the impact of VOC on the DMS photooxidation also affects the model's predictive ability for DMS oxidation products in ambient studies. In a recent indoor chamber study, Chen and Jang (2012) discovered that the MSA production from DMS photooxidation is affected by the presence of isoprene. However, kinetic studies of the impact of coexisting VOCs on DMS chemistry are inadequate.

In this study, a new DMS kinetic model was developed by including not only the most recently reported reactions and their rate constants, but also the heterogeneous reactions of DMS gaseous products on the surface of aerosol. The model was first tested for the DMSO photooxidation in the presence of NO_x using a 2 m^3 indoor chamber because DMSO is one of the important products of the DMS photooxidation. The decay of DMSO, gaseous products (e.g, dimethyl sulfone ($DMSO_2$), SO_2, NO_x and O_3) and aerosol products (e.g., MSA and H_2SO_4) were simulated using the new kinetic model integrated with the Morpho chemical solver (Jeffries et al., 1998). The resulting DMSO mechanisms have been incorporated into the kinetic mechanisms for simulating the DMS photooxidation with a few adjustments on the rate constants of the DMS related reactions. To study the influence of atmospheric VOCs on DMS oxidation, the new DMS photoxidation model coupled with the isoprene photooxidation model using the Master Chemical Mechanism (MCM) v3.2 (http://mcm.leeds.ac.uk/MCM/) was also simulated for the chamber data.

ACPD
12, 14669–14695, 2012

2 Experimental section

2.1 Indoor Teflon-film chamber experiments of photooxidation of DMSO and DMS

2.1.1 Experiment procedures

Since the DMSO oxidation mechanism is an important subset of DMS oxidation mechanism, five DMSO/NO_x experiments were conducted to validate the DMSO submodel. The experiments were operated using a 2 m^3 Teflon indoor chamber equipped with 16 UV lamps (Solarc Systems Inc., FS40T12/UVB) covering the wavelengths between 280 and 900 nm. The chamber was flushed using air from clean air generators (Aadco Model 737, Rockville, MD; Whatman Model 75-52, Haverhill, MA). DMSO was added to the chamber by passing clean air through a T union where DMSO (99.6 %, Sigma-Aldrich) was injected using a syringe and gently heated using a heat gun. NO_x (99.5 % nitric oxide, Airgas) was injected into the chamber by inserting a syringe through the injection ports. When the initial concentration of NO_x was stable, UV lamps were turned on.

The procedures of the DMS/NO_x experiments were same as those of the DMSO/NO_x experiments except that DMS (99.7 %, Aldrich) was injected into the chamber using a syringe without heating. The detailed experimental conditions for DMSO and DMS photooxidation reactions are summarized in Table 1.

2.1.2 Instrumentation and sample analysis

The concentrations of DMS, SO_2, NO_x and O_3 in the chamber were measured using an HP 5890 gas chromatography-flame ionization detector (GC-FID), a fluorescence TRS analyzer (Teledyne Model 102E), a chemiluminescence NO/NO_x analyzer (Teledyne Model 200E) and a photometric ozone analyzer (Teledyne Model 400E). Particle concentrations were measured using a scanning mobility particle sizer (SMPS,

ACPD
12, 14669–14695, 2012

TSI, Model 3080, MN) combined with a condensation nuclei counter (CNC, TSI, Model 3025A). A particle-into-liquid sampler (Applikon, ADI 2081) coupled with an ion chromatography (Metrohm, 761 Compact IC) (PILS-IC) was used to measure the major aerosol products (e.g., MSA and H_2SO_4) produced from DMS photooxidation. The detection limit of PILS-IC is 0.1 μg m^{-3} and the associated error is ±10 %.

DMSO and $DMSO_2$ were collected using a liquid N_2 (~-195 °C) trap for 8–10 minutes at a flow rate of 3 L min^{-1}. 3 ml of Acetonitrile (optima grade) with deuterated DMSO (d_6-DMSO, used as an internal standard) were then added to the trap, which was subsequently capped and immersed into hot water (~60 °C) for 10 minutes. The liquid in the trap was then transferred to a small vial for chromatography ion trap mass spectrometer (GC-ITMS, Varian model CP-3800 GC, Saturn model 2200 MS) analysis. The analysis of DMSO and $DMSO_2$ in solution using GC-ITMS has been presented by Takeuchi et al. (2010). The GC temperature profile in our study is 70 °C for 1 min; ramp to 90 °C at 5 °C min^{-1}; ramp to 280 °C at 20 °C min^{-1} and hold for 8 min. Figure S1 in the Supplement summarizes the retention time and mass spectra of DMSO, $DMSO_2$ and d_6-DMSO.

2.2 Indoor Teflon-film chamber experiments of DMS photooxidation in the presence of isoprene

Isoprene was injected into the chamber together with DMS to study its impact on DMS aerosol formation. In addition to the chemicals monitored in the DMS/NO_x experiments, major isoprene photooxidation products were sampled every 30 min (10 min sampling) for 2.5 h (5 samples in total) with a flow rate of 1.0 L min^{-1} using an impinger that contained 12 mL of acetonitrile with Bornyl Acetate (internal standard). Prior to each photoirradiation experiment, the chamber background air was analyzed for potential contamination. Further descriptions of derivatization methods for carbonyls (O-(2,3,4,5,6-Pentafluorobenzyl)-hydroxylamine hydrochloride, PFBHA) can be found elsewhere (Im et al., 2011).

ACPD
12, 14669–14695, 2012

All the impinger samples were analyzed by the GC-ITMS with the temperature program as follows: 80 °C for 1 min; ramp to 100 at 5 °C min^{-1}; hold for 3 min; ramp to 280 °C at 10 °C min^{-1} and hold for 8 min. Information for product quantification can be found elsewhere (Im et al., 2011).

3 Results and discussion

3.1 Kinetic model

3.1.1 Reaction mechanisms of DMS

DMS photooxidation in the presence of NO_x in the indoor chamber was simulated using explicit kinetic mechanisms integrated with the Morpho kinetic solver. Table S1–S3 (in the Supplement) summarize the kinetic mechanisms related to DMS oxidation along with their reaction rate constants, which were collected from the recent literature. The reaction rate constants of the oxidation for the non-sulfur compounds (e.g., formaldehyde, methanol, and methane, etc.) are obtained from the MCM mechanisms.

3.1.2 Formation of MSA and H_2SO_4 through heterogeneous reactions of gaseous DMS oxidation products

One of the major limitations of the existing explicit model for DMS photooxidation is the missing heterogeneous chemistry for DMS oxidation products in aerosol phase. In the model of this study, we assumed that DMSO produces methanesulfinic acid (MSIA), which consequently forms MSA in the aerosol phase (Bardouki et al., 2002), and $DMSO_2$ produces H_2SO_4 through heterogeneous reactions (Koga and Tanaka, 1993). In order to include heterogeneous reactions of gaseous DMS oxidation products, the rates of adsorption (k_{ad}, cm^3 molecules^{-1} s^{-1}) and desorption (k_{des}, s^{-1}) of the gaseous organic compounds (Kamens et al., 1999), have been added to the new model. The k_{ad}/k_{des} value is equal to the equilibrium constant, K_p, for the gas-particle

ACPD
12, 14669–14695, 2012

equilibrium of a given partitioning compound.

$$K_p = K_{ad}/K_{des} \quad (1)$$

The nucleation of gaseous MSA and H_2SO_4 originating from DMS photooxidation produces an aerosol mass suitable for partitioning of organic compounds. The mass of MSA and H_2SO_4 are expressed as "Aerosol" in this mechanism. The DMSO present in the gas phase is denoted as $CH_3-S(O)CH_3(g)$. In the same way, the gas phase MSIA is denoted as $CH_3-S(O)OH(g)$ and the gas phase $DMSO_2$ is denoted as $CH_3(O)S(O)CH_3(g)$. The particle phase, DMSO, MSIA, and $DMSO_2$ are described as $CH_3-S(O)CH_3(p)$, $CH_3-S(O)OH(p)$ and $CH_3(O)S(O)CH_3(p)$, respectively.

The partitioning processes of DMSO, MSIA and $DMSO_2$ are described as follows.

$$CH_3-S(O)CH_3(g) + Aerosol \rightarrow CH_3-S(O)CH_3(p) + Aerosol @ 1.1\times10^{-16}(k_{ad}) \quad (R1)$$
$$CH_3-S(O)CH_3(p) \rightarrow CH_3-S(O)CH_3(g) @ 1.7(k_{des}) \quad (R2)$$
$$CH_3-S(O)OH(g) + Aerosol \rightarrow CH_3-S(O)OH(p) + Aerosol @ 1.8\times10^{-16}(k_{ad}) \quad (R3)$$
$$CH_3-S(O)OH(p) \rightarrow CH_3-S(O)OH(g) @ 9.1\times10^{-1}(k_{des}) \quad (R4)$$
$$CH_3(O)S(O)CH_3(g) + Aerosol \rightarrow CH_3(O)S(O)CH_3(p) + Aerosol @ 2.3\times10^{-16}(k_{ad}) \quad (R5)$$
$$CH_3(O)S(O)CH_3(p) \rightarrow CH_3(O)S(O)CH_3(g) @ 7.9\times10^{-1}(k_{des}) \quad (R6)$$

The reaction of heterogeneous oxidation of DMSO, MSIA and $DMSO_2$ in aerosol are described as follows.

$$CH_3-S(O)CH_3(p) \rightarrow CH_3-S(O)OH(p) @ 8.0\times10^{3}(k_r) \quad (R7)$$
$$CH_3-S(O)OH(p) \rightarrow CH_3-SO_3H @ 2.0\times10^{3}(k_r) \quad (R8)$$
$$CH_3(O)S(O)CH_3(p) \rightarrow CH_3-SO_3H @ 2.0\times10^{-2}(k_r) \quad (R9)$$

where k_r (s^{-1}) is the rate constant for each aerosol phase reaction.

ACPD
12, 14669–14695, 2012

3.1.3 Isoprene oxidation mechanism

The kinetic mechanisms of isoprene oxidation have been described using the MCM v3.2 and compared to the data from two experiments (Exp iso-1 and Exp iso-2 in Table 2) with different NO_x concentrations.

3.2 DMS model simulation

3.2.1 Chamber characterization

The photolysis rates of inorganic species and organic compounds were calculated using the chemical solver integrated with the wavelength-dependent absorption cross-sectional areas, quantum yields, and the chamber light intensity. The light spectrum inside the chamber was measured using a spectroradiometer (PAR-NIR & UV-PAR, Apogee). For the calibration of the light intensity inside the chamber, an NO_2 photolysis experiment was separately conducted under the nitrogen gas (99.95%) environment. The detailed description of the light characterization procedure can be found in the previous study (Cao, 2008).

The chamber wall loss of oxidant gases such as O_3 and H_2O_2 were determined through several dark chamber experiments. Their wall loss rates are estimated using a first order rate constant (s^{-1}): 2.5×10^{-5} for O_3 and 6.7×10^{-4} for H_2O_2. The wall loss rate constants of DMS ($9 \times 10^{-6}\,s^{-1}$), SO_2 ($2 \times 10^{-5}\,s^{-1}$), DMSO ($6 \times 10^{-5}\,s^{-1}$) and $DMSO_2$ ($7 \times 10^{-5}\,s^{-1}$) were also experimentally determined assuming the first order rate and applied to the reaction mechanisms (Tables S1–S3) to compare the simulated results to the experimental data. Table S4 summarizes the wall loss rate constants of the compounds of this study and those found in literature (Qi et al., 2007; Ballesteros et al., 2002; Yin et al., 1990). For MSA and H_2SO_4, predominantly present in aerosol, their wall loss was calculated using the aerosol data assuming the first order decay as a function of the aerosol size (McMurry and Grosjean, 1985).

ACPD
12, 14669–14695, 2012

The background gases in the chamber, such as methane (1.8 ppm), formaldehyde (8 ppb) and acetaldehyde (2 ppb), were included in the model simulation. The methane is ubiquitous with a constant concentration. The concentrations of formaldehyde and acetaldehyde in the chamber were determined using GC-ITMS integrated with PFBHA derivatization.

3.2.2 DMSO photooxidation

Since the DMSO photooxidation mechanism is an important part of DMS photooxidation mechanisms, before the evaluation of the DMS photooxidation model, the DMSO submodel was evaluated. Five DMSO photooxidation experiments (Exp DMSO-1, Exp DMSO-2, Exp DMSO-3, Exp DMSO-4 and Exp DMSO-5 in Table 1) were conducted to confirm the DMSO submodel. The model simulation of DMSO decay, the profiles of $DMSO_2$, SO_2, NO_x and O_3 agreed with observations (Exp DMSO-1 and Exp DMSO-2 in Fig. 1). Without including the heterogeneous reactions (Reactions R2–R9), MSA concentrations are significantly underestimated. As an example, the simulations versus observation (Exp DMSO-1 and Exp DMSO-2) before and after including the heterogeneous reactions are shown in Fig. 2. Figures S2 and S3 summarize the corresponding information for Exp DMSO-3, Exp DMSO-4 and Exp DMSO-5 in Table 1. The profiles of NO_x, O_3 and SO_2 were not influenced by the heterogeneous reactions.

3.2.3 DMS photooxidation

The DMSO submodel that contains heterogeneous reactions of DMS products is included in the DMS oxidation mechanism. The new DMS model was simulated against five DMS photooxidation experiments. In the model of this study, the reaction of DMS with the $CH_3S\cdot$ radical, the decomposition of the $CH_3\text{-}SO_3\cdot$ radical and the reaction of the $CH_3(O)S(O)\cdot$ radical with NO_2 were also included. These reactions have been either missed or assigned with improper estimates of reaction rate constants in the ex-

ACPD
12, 14669–14695, 2012

isting models. The prediction of DMS decay and DMS product formation are improved after modification of the reactions.

Barnes et al. (1988) proposed the DMS + $CH_3S\cdot$ reaction in order to explain the fast decay of DMS in the presence of NO_x. It was found that, without this reaction, the model simulation of DMS decay is systematically slower than observation. The DMS + $CH_3S\cdot$ reaction (Reaction No. 103 in Table S2) was thus added to the model with an estimated rate constant so that the decay of DMS and the profiles of NO_x and O_3 of the simulation result could be best fitted to that of observation in our study.

The reaction rate constant of decomposition of the CH_3-$SO_3\cdot$ radical (reaction No. 46 in Table S1) was previously estimated to be 0.16 s^{-1} without experimental confirmation (Yin et al., 1990). In this study, it was found that the change of this rate constant does not significantly influence the DMS decay or the NO_x profile; rather, it impacts the distribution of H_2SO_4 and MSA. A value of 0.04 s^{-1} was found to best fit the measured concentrations of aerosol-phase H_2SO_4 and MSA.

The rate constant of the reaction between the $CH_3(O)S(O)\cdot$ radical and NO_2 (reaction No. 24 in Table S1) was reported to be $(2.2\pm1.1)\times10^{-12}$ cm^3 $molecule^{-1}$ s^{-1} (Ray et al., 2010) with one standard deviation of error. In this study, a value of 5×10^{-13} (within two standard deviation of error of Ray's data) was found to best fit the SO_2 and acid formation profile.

The major gaseous products of DMS oxidation were simulated and are shown in Fig. 3a (for Exp DMS-3, Exp DMS-4 and Exp DMS-5) and Fig. S4A (for Exp DMS-1 and Exp DMS-2). In general, SO_2 and $DMSO_2$ were reasonably predicted. The measured DMSO concentrations in the experiments containing DMS were not reported in this study (see "The artifacts of DMSO measurement in the presence of DMS" section in the supplementary materials).

For aerosol-phase products, the model underestimated the concentrations of MSA and H_2SO_4 by up to a factor of three during the first 60 min of chamber experiments, but simulated closer to the measurements during the rest of the experiments (Figs. 3c and S4c). In the model, heterogeneous reactions associated with DMSO,

ACPD
12, 14669–14695, 2012

MSIA, and $DMSO_2$ are controlled by partitioning processes that are governed mainly by the aerosol mass. However, in the early stage of the experiment, aerosols are small because they are formed via nucleation, so their surface area would be much more important than their mass in the partitioning processes. The model's predictions limit the accommodation of DMSO, MSIA, and $DMSO_2$ due to the mass-based partitioning processes in the model. Consequently, the production of MSA and sulfuric acid in the early stage of the chamber experiments was underpredicted in the model of this study.

3.3 Impact of the coexisting isoprene on DMS photooxidation

3.3.1 Isoprene photooxidation

The MCM v3.2 includes comprehensive isoprene photooxidation mechanisms including some very recently proposed mechanisms such as epoxide formation (Paulot et al., 2009). The isoprene model was simulated against Exp iso-1 and Exp iso-2. The major products (e.g., methacrolein (P1), methyl vinyl ketone (P2), glyoxal (P3), and methylglyoxal (P4)) originating from isoprene were also simulated and compared to the experimentally measured concentrations. The mass spectra data for isoprene's major gaseous products are summarized in Fig. S5 in the Supplement and the simulation results are illustrated against observation in Fig. S6 in the Supplement. Overall, the MCM mechanism predicts the isoprene decay, the formation of several isoprene products and the profiles of NO_x and O_3 well.

3.3.2 DMS photooxidation with coexisting isoprene

Experiments iso-DMS-1, iso-DMS-2 and iso-DMS-3 were carried out under similar initial concentrations of DMS and NO_x. The simulation profiles of DMS, isoprene, MSA and H_2SO_4 are shown in Fig. 4 in comparison with the measurements. The concentrations of NO_x, O_3 and the gas phase products (P1–P4) originating from isoprene oxidation are well predicted using the kinetic model (Fig. S7 in the Supplement).

ACPD
12, 14669–14695, 2012

To understand the impact of isoprene on the production of MSA and H_2SO_4, molar yields (defined as the amount of a produced product divided by the amount of the consumed DMS) of MSA and H_2SO_4 were compared between experiments with different initial isoprene concentrations with similar amounts of DMS consumption. The yields of MSA and H_2SO_4 (in Table 3) were found to increase as the initial isoprene increases for both the model simulation and experimental data (after correction for wall loss and chamber dilution).

To understand the impact of isoprene on yields of MSA and H_2SO_4, the contribution of gas-phase reactions and aerosol-phase heterogeneous chemistry of DMS photooxidation to the formation of MSA and H_2SO_4 were analyzed using the integrated reaction rate (IRR) as shown in Table 3. The integrated reaction rate, expressed as an accumulated flux of chemical formation or consumption at a given reaction and an initial concentration, is estimated using the Morpho chemical solver. Overall, the IRR values of the formation of both MSA and H_2SO_4 increase with the increasing initial isoprene concentration.

The IRR analysis suggests that higher initial isoprene concentrations enhance the formation of SO_2, consequently increasing the production of H_2SO_4. The IRR (Table S5) of DMS with $O(^3P)$ was found to be the major variant among the experiments with different levels of isoprene concentration. The coexisting isoprene efficiently increases NO_x cycles during DMS photooxidation and also increases the reaction of DMS with $O(^3P)$ (Reaction No. 61 in Table S2), producing a CH_3-SO· radical with a unity yield. The resulting CH_3-SO· is efficiently oxidized into a $CH_3(O)S(O)$· radical that is known to be a critical intermediate for the formation of SO_2 and MSA (Yin et al., 1990).

The effect of isoprene on MSA production is complicated because isoprene influences both gas-phase reactions and heterogeneous reactions. Similarly to H_2SO_4, MSA formation in the gas phase is increased with higher isoprene concentrations due to the higher production of the $CH_3(O)S(O)$· radical. The MSA and H_2SO_4 produced

ACPD
12, 14669–14695, 2012

in the gas phase reaction synergetically increase the pathway to the MSA formation in the aerosol through heterogeneous reactions of DMS oxidation products.

Although the newly built DMS kinetic model of this study successfully predicts the trend (Table 3) in the yields of MSA and H_2SO_4 under different initial isoprene concentrations, the model's predictions somewhat deviate from experimental data when the isoprene concentration is high. Similarly, for Exp iso-DMS-1, Exp iso-DMS-2 and Exp iso-DMS-3 in Fig. 4, the model underpredicts MSA concentrations. The gap between measurement and prediction increases as the initial isoprene concentration increases. It is expected that the secondary organic aerosol (SOA) formed from isoprene photooxidation would influence the formation of MSA, possibly because the SOA might increase the solubility of DMS products such as DMSO. The heterogeneous chemistry on SOA is not included in this study and this may possibly lead to the deviation of the model's predictions from experimental data.

3.4 Potential application of the kinetic model in ambient simulation

To evaluate the model's performance for lower concentrations of isoprene and DMS, Exp iso-DMS-4 and Exp iso-DMS-5 were conducted. The simulation accords well with measurements (Fig. 5) for both gas-phase and aerosol-phase products, suggesting that the newly constructed DMS kinetic model could potentially be suitable for ambient simulation.

4 Conclusion and atmospheric implication

In this study, the modeling of DMS oxidation mechanisms has been advanced by including both the most recent reaction rate constants and heterogeneous reactions of gas-phase DMS oxidation products in the aerosol. The newly constructed kinetic model closely matches the experimental data for the DMS decay and time profiles of NO_x, O_3, SO_2 and $DMSO_2$. The prediction of H_2SO_4 and MSA concentrations has been signif-

ACPD
12, 14669–14695, 2012

icantly improved by the model of this study as compared with models that neglect heterogeneous reactions of gaseous DMS oxidation products.

The MSA production appeared to be increased as the initial isoprene concentration increased. The IRR analysis in the model suggests that the presence of isoprene increases NO_x cycles during the DMS photooxidation. Subsequently, the reaction of DMS with $O(^3P)$ is enhanced, eventually causing higher yields of MSA and H_2SO_4 through gas-phase reactions. With greater production of MSA and H_2SO_4 in the presence of high concentrations of isoprene, the heterogeneous reactions of DMSO and MSIA were also enhanced, in turn producing more MSA. The formation of isoprene SOA may also increase the yields of MSA and H_2SO_4 through some unknown mechanisms via heterogeneous reactions of DMS oxidation products.

To apply the model to the reaction in ambient air, further investigation is needed, not only to understand the detailed mechanisms of aerosol formation from DMS oxidation in the presence of SOA, but also to improve the model for SOA production in the presence of DMS. In addition, Zhu et al. (2006) indicated that the OH· radical reaction with MSA consumes almost 20 % of MSA and produces about 8 % of H_2SO_4within 3 days under typical marine atmospheric conditions. In this study, due to the short duration (~3 hours), the MSA decay might be insignificant. However, this should be considered when the model is applied to the reactions in the ambient air. Similar to the MSA production through heterogeneous reactions of DMSO, SO_2 can be oxidized on the surface of aerosol but will not be significant because of its low reactivity with oxidants (e.g., OH radical). However, in the ambient air, the heterogeneous production of H_2SO_4 through SO_2 reactions on aerosol should be considerable especially in the presence of atmospheric catalysts such as iron ions (Freiberg, 1974).

Supplementary material related to this article is available online at: http://www.atmos-chem-phys-discuss.net/12/14669/2012/acpd-12-14669-2012-supplement.pdf.

ACPD
12, 14669–14695, 2012

Acknowledgements. This work was supported by grants from the National Science Foundation (ATM-0852747) and the Alumni Scholarship from the University of Florida. Publication of this article was funded in part by the University of Florida Open-Access Publishing Fund.

References

Atkinson, R., Baulch, D. L., Cox, R. A., Hampson, R. F., Kerr, J. A., and Troe, J.: Evaluated Kinetic and Photochemical Data for Atmospheric Chemistry. 3. Iupac Subcommittee on Gas Kinetic Data Evaluation for Atmospheric Chemistry, J. Phys. Chem. Ref. Data., 18, 881–1097, 1989. 14671

Atkinson, R., Baulch, D. L., Cox, R. A., Hampson, R. F., Kerr, J. A., Rossi, M. J., and Troe, J.: Evaluated kinetic and photochemical data for atmospheric chemistry: Supplement VI – IUPAC subcommittee on gas kinetic data evaluation for atmospheric chemistry, J. Phys. Chem. Ref. Data, 26, 1329–1499, 1997. 14671

Balla, R. J. and Heicklen, J.: Oxidation of Sulfur Compounds.2.Thermal Reactions of NO_2 with Aliphatic Sulfur-Compounds, J. Phys. Chem.-US, 88, 6314–6317, 1984. 14671

Ballesteros, B., Jensen, N. R., and Hjorth, J.: FT-IR study of the kinetics and products of the reactions of dimethylsulphide, dimethylsulphoxide and dimethylsulphone with Br and BrO, J. Atmos. Chem., 43, 135–150, 2002. 14677

Bardouki, H., da Rosa, M. B., Mihalopoulos, N., Palm, W. U., and Zetzsch, C.: Kinetics and mechanism of the oxidation of dimethylsulfoxide (DMSO) and methanesulfinate (MSI^-) by OH radicals in aqueous medium, Atmos. Environ., 36, 4627–4634, 2002. 14672, 14675

Bardouki, H., Berresheim, H., Vrekoussis, M., Sciare, J., Kouvarakis, G., Oikonomou, K., Schneider, J., and Mihalopoulos, N.: Gaseous (DMS, MSA,SO_2, H_2SO_4 and DMSO) and particulate (sulfate and methanesulfonate) sulfur species over the northeastern coast of Crete,, J. Phys. Chem.-US, 3, 1871–1886, 2003. 14670

Barnes, I., Bastian, V., and Becker, K. H.: Kinetics and Mechanisms of the Reaction of Oh Radicals with Dimethyl Sulfide, Int. J Chem. Kinet., 20, 415–431, 1988. 14679

Barnes, I., Hjorth, J., and Mihalopoulos, N.: Dimethyl sulfide and dimethyl sulfoxide and their oxidation in the atmosphere, Chem. Rev., 106, 940–975, 2006. 14671

Barone, S. B., Turnipseed, A. A., and Ravishankara, A. R.: Role of adducts in the atmospheric oxidation of dimethyl sulfide, Faraday Discuss., 100, 39–54, 1995. 14670

ACPD

12, 14669–14695, 2012

Cao, G.: Secondary organic aerosol formation from toluene oxidation in the presence of inorganic aerosols, Ph.D. dissertation, Department of Environmental Sciences and Engineering, 2008. 14677

Charlson, R. J., Lovelock, J. E., Andreae, M. O., and Warren, S. G.: Oceanic Phytoplankton, Atmospheric Sulfur, Cloud Albedo and Climate, Nature, 326, 655–661, 1987. 14670

Chen, G., Davis, D. D., Kasibhatla, P., Bandy, A. R., Thornton, D. C., Huebert, B. J., Clarke, A. D., and Blomquist, B. W.: A study of DMS oxidation in the tropics: Comparison of christmas island field observations of DMS, SO_2, and DMSO with model simulations, J. Atmos. Chem., 37, 137–160, 2000. 14671

Chen, T. and Jang, M.: Secondary organic aerosol formation from photooxidation of a mixture of dimethyl sulfide and isoprene, Atmos. Environ., 46, 271–278, 2012. 14672

Davis, D., Chen, G., Bandy, A., Thornton, D., Eisele, F., Mauldin, L., Tanner, D., Lenschow, D., Fuelberg, H., Huebert, B., Heath, J., Clarke, A., and Blake, D.: Dimethyl sulfide oxidation in the equatorial Pacific: Comparison of model simulations with field observations for DMS, SO_2, H_2SO_4(g), MSA(g), MS, and NSS, J. Geophys. Res.-Atmos., 104, 5765–5784, 1999. 14671

Freiberg, J.: Effects of Relative Humidity and Temperature on Iron-Catalyzed Oxidation of SO_2 in Atmospheric Aerosols, Environ. Sci. Technol., 8, 731–734, 1974. 14683

Gaston, C. J., Pratt, K. A., Qin, X. Y., and Prather, K. A.: Real-Time Detection and Mixing State of Methanesulfonate in Single Particles at an Inland Urban Location during a Phytoplankton Bloom, Environ. Sci. Technol., 44, 1566–1572, 2010. 14670

Im, Y., Jang, M., Delcomyn, C. A., Henley, M. V., and Hearn, J. D.: The effects of active chlorine on photooxidation of 2-methyl-2-butene, Sci. Total. Environ., 409, 2652–2661, 2011. 14674, 14675

Jeffries, H., Gary, M., Kessler, M., and Sexton, K.: Morphecule reaction mechanism, MORPHO, ALLOMORPHIC., simulation software, http://airsite.unc.edu/atmchemunc/morpho/intro.html, 1998. 14672

Kamens, R., Jang, M., Chien, C. J., and Leach, K.: Aerosol formation from the reaction of alpha-pinene and ozone using a gas phase kinetics aerosol partitioning model, Environ. Sci. Technol., 33, 1430–1438, 1999. 14675

Koga, S. and Tanaka, H.: Numerical Study of the Oxidation Process of Dimethylsulfide in the Marine Atmosphere, J. Atmos. Chem., 17, 201–228, 1993. 14675

ACPD

12, 14669–14695, 2012

Lucas, D. D. and Prinn, R. G.: Mechanistic studies of dimethylsulfide oxidation products using an observationally constrained model, J. Geophys. Res.-Atmos., 107, 1–26, 2002. 14671
Lukács, H., Gelencsér, A., Hoffer, A., Kiss, G., Horváth, K., and Hartyáni, Z.: Quantitative assessment of organosulfates in size-segregated rural fine aerosol, Atmos. Chem. Phys., 9, 231–238, doi:10.5194/acp-9-231-2009, 2009. 14670
McMurry, P. H. and Grosjean, D.: Gas and Aerosol Wall Losses in Teflon Film Smog Chambers, Environ. Sci. Technol., 19, 1176–1182, 1985. 14677
Mihalopoulos, N., Kerminen, V. M., Kanakidou, M., Berresheim, H., and Sciare, J.: Formation of particulate sulfur species (sulfate and methanesulfonate) during summer over the Eastern Mediterranean: A modelling approach, Atmos. Environ., 41, 6860–6871, 2007. 14672
Paulot, F., Crounse, J., Kjaergaard, H., Kurten, A., St Clair, J., Seinfeld, J., and Wennberg, P.: Unexpected Epoxide Formation in the Gas-Phase Photooxidation of Isoprene, Science, 325, 730–733, 2009. 14680
Qi, B., Chao, Y. T., and Chen, Z. M.: Mechanism and kinetics of the production of hydroxymethyl hydroperoxide in ethene/ozone/water gas-phase system, Sci. China Series B-Chem., 50, 425–431, 2007. 14677
Ray, A., Vassalli, I., Laverdet, G., and LeBras, G.: Kinetics of the thermal decomposition of the CH_3SO_2 radical and its reaction with NO_2 at 1 torr and 298 K, J. Phys. Chem. USA, 107, 6640–6645, 2010. 14679
Sander, S., Friedl, R., Golden, D., Kurylo, M., Moortgat, G., Wine, P., Ravishankara, A. R. Kolb, C., Molina, M., Finlayson-Pitts, B. J., and Huie, R.: Chemical kinetics and photochemical data for use in atmospheric studies. Evaluation Number 15, JPL Publication, 06-2, 1–523, 2006. 14671
Takeuchi, A., Yamamoto, S., Narai, R., Nishida, M., Yashiki, M., Sakui, N., and Namera, A.: Determination of dimethyl sulfoxide and dimethyl sulfone in urine by gas chromatography-mass spectrometry after preparation using 2,2-dimethoxypropane, Biomed. Chromatogr., 24, 465–471, 2010. 14674
Turnipseed, A. and Ravishankara, A.: The atmospheric oxidation of dimethylsulfide: elementary steps in a complex mechanism, in : G. Restelli and G. Angeletti (eds), Dimethylsulfide:Oceans, Atmosphere and Climate, Kluwer Acad. Publ., Dordrecht, Norwell, Mass., 185–195, 1993. 14671
Urbanski, S. P. and Wine, P. H.: Chemistry of gas phase organic sulfur-centred radicals, edited by: Alfassi, Z. B., John Wiley and Sons, 97–140, 1999. 14671

ACPD
12, 14669–14695, 2012

Yin, F. D., Grosjean, D., and Seinfeld, J. H.: Photooxidation of Dimethyl Sulfide and Dimethyl Disulfide.1. Mechanism Development, J. Atmos. Chem., 11, 309–364, 1990. 14671, 14677, 14679, 14681

Zhu, L., Nenes, A., Wine, P. H., and Nicovich, J. M.: Effects of aqueous organosulfur chemistryon particulate methanesulfonate to non-sea salt sulfate ratios in the marine atmosphere, J.Geophys. Res.-Atmos., 111, D05316, doi:10.1029/2005JD006326, 2006. 14683

ACPD

12, 14669–14695, 2012

Table 1. Chamber experiments of the photooxidation of DMS and DMSO in the presence of NO_x.

Exp	Temp, °C	RH %	Initial sulfur conc., ppb	Initial NO_x conc., ppb
DMSO-1	22	24	291.3	49.1
DMSO-2	22	26	306.5	199.1
DMSO-3	21	23	99.1	33.0
DMSO-4	24	24	170.0	85.1
DMSO-5	26	27	75.7	33.0
DMS-1	24	28	714.0	103.7
DMS-2	26	28	210.0	203.3
DMS-3	25	28	146.0	26.4
DMS-4	27	40	134.0	21.7
DMS-5	25	60	161.0	81.0

ACPD
12, 14669–14695, 2012

Table 2. Chamber experimental conditions for isoprene photooxidation with and without DMS.

Exp	Temp, °C	RH %	Initial DMS conc., ppb	Initial isoprene conc., ppb	Initial NO_x conc., ppb
iso-1	24.5	30	0	644	76.9
iso-2	25.0	32	0	600	26.7
iso-DMS-1	23.5	28	243	560	84.8
iso-DMS-2	23.2	30	265	1360	84.5
iso-DMS-3	23.0	30	276	2248	65.9
iso-DMS-4	22.0	10	31	210	40.3
iso-DMS-5	23.1	30	20[a]	40[a]	15.6

Initial DMS and isoprene concentrations in iso-DMS-5 were estimated based on the amount of injected chemicals due to the instrumental detection limit.

ACPD
12, 14669–14695, 2012

Table 3. Model simulation of the yields of MSA and H_2SO_4 and the integrating reaction rates (IRR) of the formation of MSA and H_2SO_4 in the presence of different amount of isoprene.

Exp	Isoprene	Sim. time[c],	ΔDMS,	Molar yield[d]		IRR normalized by ΔDMS[b]			
						MSA		H_2SO_4	
	ppb	min	ppb	MSA	H_2SO_4	gas pathway[e]	aerosol pathway[f]	gas pathway[e]	aerosol pathway[f]
iso-DMS-1	560	44	6.4	9.70 % (8.05 %)	0.89 % (1.96 %)	0.092	0.001	0.008	0
iso-DMS-2	1360	50	5.9	11.02 % (9.80 %)	1.02 % (2.00 %)	0.108	0.002	0.010	0
iso-DMS-3	2248	163	6.0	11.36 % (20.79 %)	1.54 % (2.34 %)	0.110	0.015	0.015	0

[a] All the reported results (except those in brackets) in this table were based on the model simulation. The experimental yield data are in the brackets. The MSA yields in this table were calculated using the data from Fig. 4 with corrections for DMS wall loss and chamber dilution. Note that the DMS decay in Fig. 4 contains the decay due to photooxidation, wall loss and chamber dilution. [b] Refer to 3.3.1 for the description of IRR. [c] The simulation time was set so that the consumed DMS was fixed at around 6 ppb for fair comparison among different systems. [d] Molar yield is defined as the amount of MSA (or H_2SO_4) formed divided by the amount (around 6 ppb) of DMS consumed. [e] The IRR for Reaction No. 48 and 54 in Table S1 and Reaction No. 132 in Table S2 in the Supplement were added up for MSA formation while the IRR for Reaction No. 170 and 171 in Table 3 were added up for H_2SO_4 formation. [f] The IRR for MSA formation was based on Reaction (R8) in Sect. 3.1.2 and that for H_2SO_4 formation was from Reaction (R9) in the same section.

ACPD
12, 14669–14695, 2012

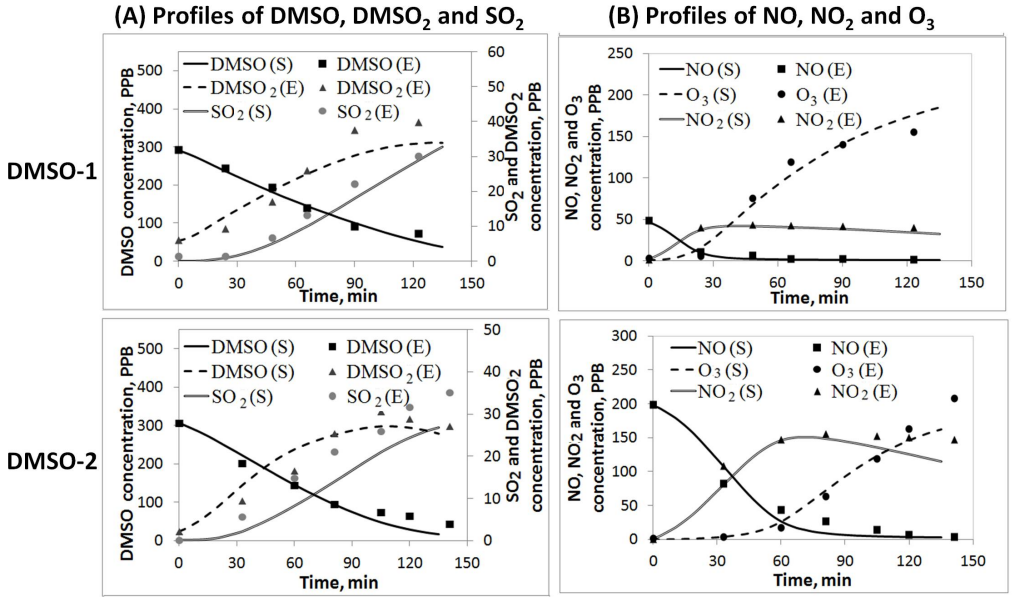

Fig. 1. The time profiles of DMSO, $DMSO_2$, SO_2, NO_x and O_3 for the photooxidation of DMSO in the presence of NO_x (Exp DMSO-1 and DMSO-2 in Table 1). "E" denotes the experimentally observed concentrations of chemical species and "S" for those simulated using the kinetic model.

ACPD
12, 14669–14695, 2012

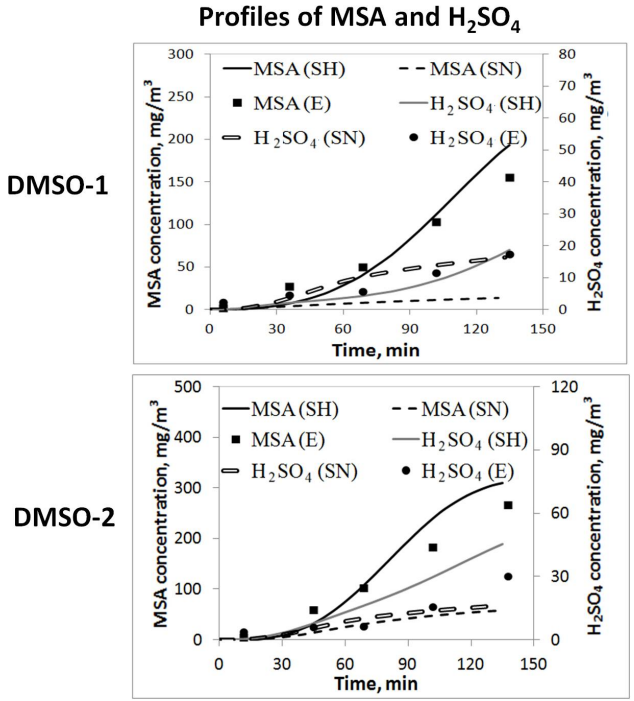

Fig. 2. Model simulation of MSA and sulfuric acid for the photooxidation of DMSO in the presence of NO_x (Exp DMSO-1 and DMSO-2 in Table 1) with (SH) and without (SN) including heterogeneous reactions. The experimentally observed concentrations (E) of MSA and H_2SO_4 are shown as comparison.

ACPD
12, 14669–14695, 2012

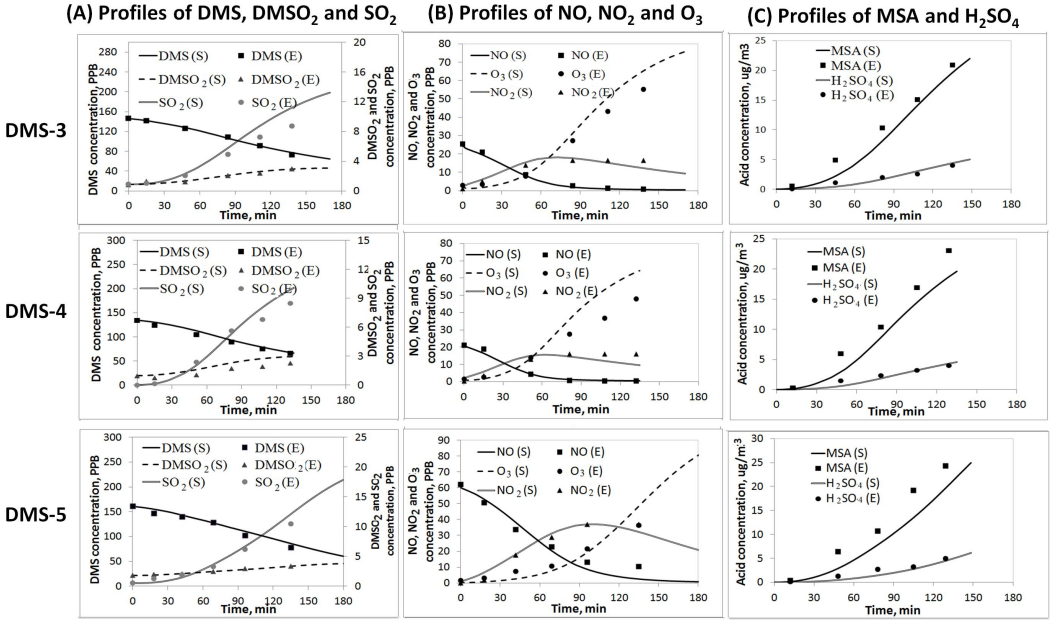

Fig. 3. The time profiles of DMS, $DMSO_2$, SO_2, MSA, sulfuric acid, NO_x and O_3 for the photooxidation of DMSO in the presence of NO_x (Exp DMS-3, Exp DMS-4 and Exp DMS-5 in Table 1). "E" denotes the experimentally observed concentrations of chemical species and "S" for those simulated using the kinetic model.

ACPD
12, 14669–14695, 2012

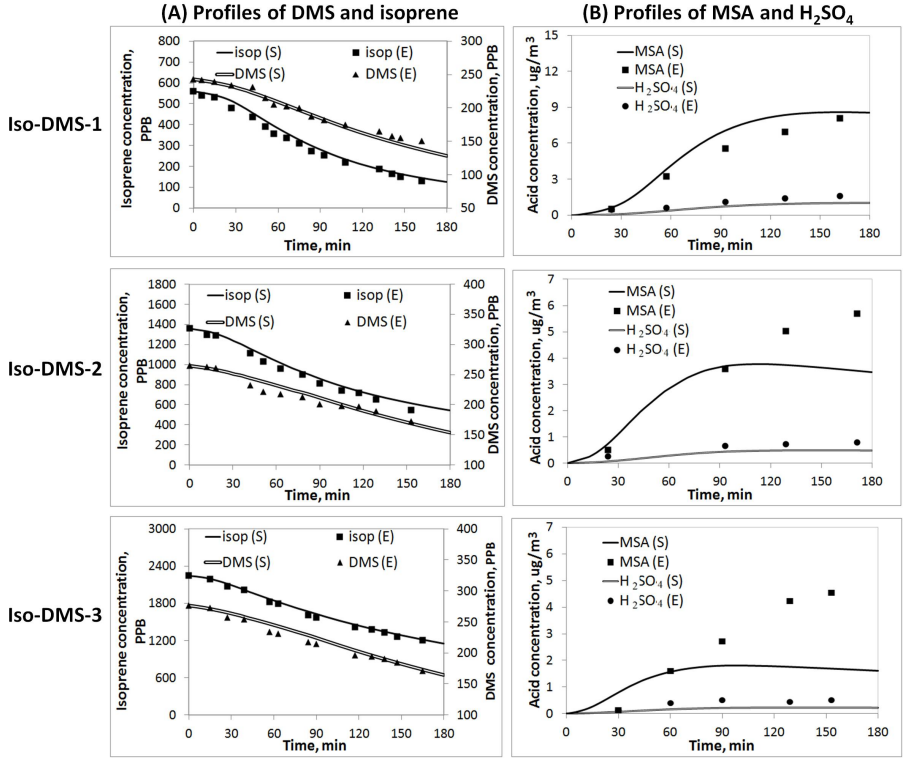

Fig. 4. The time profiles of isoprene, DMS, MSA and sulfuric acid for the photooxidation of DMS and NO_x in the presence of 560 ppb (Exp iso-DMS-1), 1360 ppb (Exp iso-DMS-2), and 2248 ppb (Exp iso-DMS-3) of isoprene. "E" denotes the experimentally observed concentrations of chemical species and "S" for those simulated using the kinetic model. The decay of DMS and isoprene was not corrected for the wall loss and chamber dilution while the production of MSA and sulfuric acid was corrected for both the wall loss and chamber dilution.

ACPD
12, 14669–14695, 2012

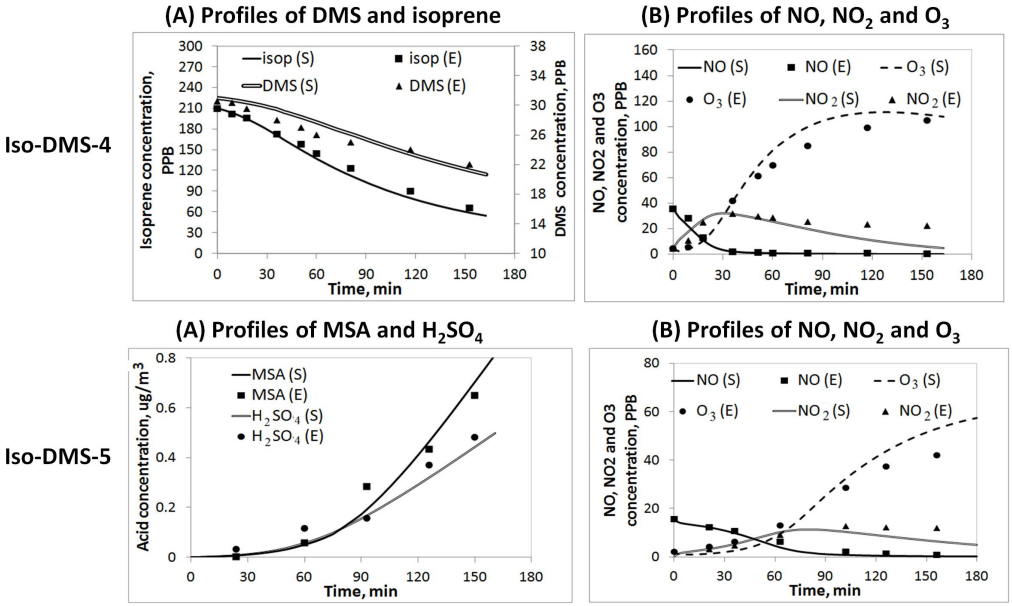

Fig. 5. The time profiles of Exp iso-DMS-4 (isoprene, DMS, NO_x and O_3 from the photooxidation of 31 ppb of DMS and 40 ppb of NO_x in the presence of 210 ppb of isoprene) and time profiles for Exp iso-DMS-5 (NO_x, O_3, MSA and H_2SO_4 from 20 ppb of DMS and 15 ppb of NO_x in the presence of 40 ppb of isoprene). "E" denotes the experimentally observed concentrations of chemical species and "S" for those simulated using the kinetic model.

ACPD
12, 14669–14695, 2012